

# Noncovalent and Covalent O–H...O Interactions in PPh<sub>3</sub>O Cocrystals: A Correlation Study Involving QTAIM, SAPT, NBO, and IBSI Methods

Suphal Sen, Ankita Sinha, Suparna Banerjee, Snehasish Debnath, Aniruddha Ghosh, Jishnunil Chakraborty,\* and Jaydip Gangopadhyay\*



Cite This: *ACS Omega* 2024, 9, 22476–22487



Read Online

ACCESS |

Metrics & More

Article Recommendations

Supporting Information

**ABSTRACT:** PPh<sub>3</sub>O.hemihydrate polymorphs and 11 assorted PPh<sub>3</sub>O cocrystals collectively constitute a reliable stock to pursue a systematic analysis aiming to investigate the impacts of some vital issues on the TPPO.H-bond donor aggregates. The issues highlighted herein are (i) effect of varying acidity of H-bond donors on the degeneracy of lone pairs of the H-bond acceptor (PPh<sub>3</sub>O), (ii) effectiveness of the  $|V(r)|/G(r)$  and  $H(r)/\rho(r)$  parameters as a covalency metric, (iii) 3c–4e bonding in the covalent PPh<sub>3</sub>O.nitric acid cocrystal, (iv) salient features of H-bond interaction energy and an interplay of its components, (v) an intrinsic bond strength scale for the PPh<sub>3</sub>O cocrystals, and (vi) reliable empirical relations between several bond descriptors for a quick estimation of interaction energy. To be specific about point (vi), we have propounded two promising avenues for a fast semiquantitative calculation of interaction energy from an endearing nonenergetic parameter, viz., bond length:  $d_{\text{O} \cdots \text{H} \cdots \text{O}} \rightarrow \rho_{\text{BCP}}$  (MAPE = 2.36%)  $\rightarrow E_{\text{SAPT0}}$  (MAPE = 9.26%), and  $d_{\text{O} \cdots \text{H} \cdots \text{O}} \rightarrow \text{IBSI}$  (MAPE = 1.87%)  $\rightarrow E_{\text{SAPT0}}$  (MAPE = 9.66%). All the aforesaid issues have been explored in detail through the QTAIM, NBO, and IBSI analyses (M06-2X-D3/def2-TZVP level), as well as by the SAPT study at the SAPT0/aug-cc-pVDZ platform. The statistically valid correlation studies can be particularly conducive for practical purposes as a transformative extension of the established facts into postulates for the unknown cocrystals.

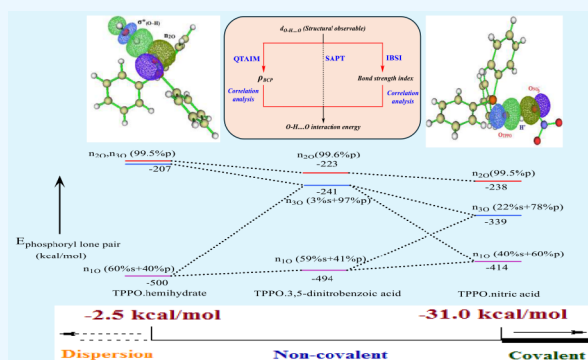


**Table 1. QTAIM Descriptors Computed at M06-2X-D3/def2-TZVP Level at the BCPs of the 17 Intermolecular O–H...O Interactions in TPPO.hemihydrate Polymorphs and 11 Structurally Characterized TPPO Cocrystals<sup>a</sup>**

TPPO cocrystals	$\rho(r)$ (a.u.)	$\nabla^2\rho(r)$ (a.u.)	$V(r)$ (a.u.)	$G(r)$ (a.u.)	$ V(r) /G(r)$	$H(r)$ (a.u.)	$H(r)/\rho(r)$
TPPO.nitric acid <sup>19</sup>	0.1044	-0.0081	-0.1185	0.0582	2.036	$-6.02 \times 10^{-2}$	-0.5766
TPPO.p-nitrophenol <sup>17</sup>	0.0653	0.1085	-0.0715	0.0493	1.450	$-2.22 \times 10^{-2}$	-0.3399
TPPO.3,5-dinitrobenzoic acid <sup>22</sup>	0.0629	0.1219	-0.0706	0.0505	1.398	$-2.00 \times 10^{-2}$	-0.3179
TPPO.1-naphthoic acid <sup>15</sup>	0.0524	0.1455	-0.0585	0.0474	1.234	$-1.11 \times 10^{-2}$	-0.2118
TPPO.dephenylmethanol <sup>23</sup>	0.0514	0.1015	-0.0521	0.0387	1.346	$-1.33 \times 10^{-2}$	-0.2587
TPPO.3-chlorobenzoic acid <sup>16</sup>	0.0331	0.1546	-0.0342	0.0364	0.939	$2.23 \times 10^{-3}$	0.0674
TPPO.pentafluorophenol <sup>21</sup>	0.0315	0.1440	-0.0314	0.0337	0.932	$2.28 \times 10^{-3}$	0.0724
TPPO.hydroquinone <sup>14</sup>	0.0299	0.1360	-0.0290	0.0315	0.921	$2.49 \times 10^{-3}$	0.0833
TPPO.trimethylphenylboronic acid <sup>13</sup>	0.0276	0.1412	-0.0269	0.0311	0.865	$4.18 \times 10^{-3}$	0.1514
TPPO.6-chloro-2-pyridinol <sup>20</sup>	0.0283	0.1432	-0.0277	0.0318	0.871	$4.02 \times 10^{-3}$	0.1420
TPPO.hydrogenperoxide <sup>18</sup>	0.0287	0.1319	-0.0272	0.0301	0.904	$2.88 \times 10^{-3}$	0.1003
TPPO.hydrogenperoxide <sup>18</sup>	0.0272	0.1246	-0.0249	0.0280	0.889	$3.10 \times 10^{-3}$	0.1139
TPPO.hydroquinone <sup>14</sup>	0.0259	0.1188	-0.0235	0.0266	0.883	$3.11 \times 10^{-3}$	0.1201
TPPO.hemihydrate ( <i>Fdd2</i> ) <sup>a</sup>	0.0234	0.1004	-0.0198	0.0224	0.884	$2.64 \times 10^{-3}$	0.1128
TPPO.hemihydrate ( <i>C2/c</i> ) <sup>10</sup>	0.0162	0.0806	-0.0118	0.0159	0.742	$4.15 \times 10^{-3}$	0.2562
TPPO.hemihydrate ( <i>Cc</i> ) <sup>11</sup>	0.0167	0.0843	-0.0127	0.0169	0.751	$4.17 \times 10^{-3}$	0.2497
TPPO.hemihydrate ( <i>Cc</i> ) <sup>11</sup>	0.0161	0.0786	-0.0117	0.0156	0.750	$3.97 \times 10^{-3}$	0.2465

<sup>a</sup>Geometrical attributes have been taken from our unpublished X-ray structure of orthorhombic TPPO.hemihydrate polymorph (CCDC No. 2281529).

**Table 2. Energy Components (SAPT0/aug-cc-pVDZ, kcal/mol) and Geometrical Attributes of 4 O–H...O Interactions in the TPPO.hemihydrate Polymorphs and 13 O–H...O Interactions in 11 TPPO Cocrystals<sup>a</sup>**

TPPO cocrystals	O–H...O bond attributes (Å, °)	$E_{\text{elst}}$	$E_{\text{exch}}$	$E_{\text{ind}}$	$E_{\text{dis}}$	$E_{\text{SAPT0}}$
TPPO.nitric acid	1.352, 142.99	-39.82 (44.9)	46.22	-38.37 (43.4)	-10.31 (11.7)	-42.28
TPPO.p-nitrophenol	1.539, 165.95	-28.07 (52.0)	29.05	-16.98 (31.5)	-8.87 (16.5)	-24.87
TPPO.3,5-dinitrobenzoic acid	1.554, 169.82	-29.71 (54.4)	27.75	-15.09 (27.6)	-9.82 (17.9)	-26.87
TPPO.1-naphthoic acid	1.602, 170.02	-21.74 (55.1)	21.27	-10.81 (27.4)	-6.90 (17.5)	-18.18
TPPO.dephenylmethanol	1.626, 146.23	-21.25 (44.9)	26.11	-12.63 (26.8)	-13.40 (28.3)	-21.17
TPPO.3-chlorobenzoic acid	1.766, 170.44	-17.06 (60.7)	13.25	-5.58 (19.9)	-5.45 (19.4)	-14.84
TPPO.pentafluorophenol	1.792, 173.70	-16.73 (59.8)	12.88	-5.35 (19.1)	-5.92 (21.1)	-15.12
TPPO.hydroquinone	1.817, 169.68	-14.45 (56.4)	12.07	-4.75 (18.6)	-6.40 (25.0)	-13.53
TPPO.trimethylphenylboronic acid	1.838, 167.64	-13.87 (48.9)	13.06	-4.27 (15.1)	-10.21 (36.0)	-15.29
TPPO.6-chloro-2-pyridinol	1.842, 161.64	-13.77 (53.3)	13.12	-4.19 (16.2)	-7.87 (30.5)	-12.71
TPPO.hydrogenperoxide	1.850, 163.96	-13.16 (63.4)	10.47	-3.72 (17.9)	-3.88 (18.7)	-10.29
TPPO.hydrogenperoxide	1.870, 177.11	-13.63 (63.7)	10.06	-3.71 (17.3)	-4.07 (19.0)	-11.35
TPPO.hydroquinone	1.874, 174.96	-13.46 (55.7)	10.38	-4.32 (17.9)	-6.39 (26.4)	-13.79
TPPO.hemihydrate ( <i>Fdd2</i> )	1.911, 171.83	-10.80 (64.8)	7.42	-3.09 (18.5)	-2.78 (16.7)	-9.25
TPPO.hemihydrate ( <i>C2/c</i> )	2.040, 173.96	-7.53 (67.2)	4.08	-1.72 (15.3)	-1.96 (17.5)	-7.13
TPPO.hemihydrate ( <i>Cc</i> )	2.054, 156.08	-8.18 (68.5)	4.75	-1.64 (13.7)	-2.12 (17.8)	-7.19
TPPO.hemihydrate ( <i>Cc</i> )	2.084, 158.03	-8.22 (68.7)	4.60	-1.63 (13.6)	-2.12 (17.7)	-7.37

<sup>a</sup>Values in the parentheses give the percentage contribution of that energy component to the total stabilization energy emerging from electrostatic, induction, and dispersion forces.

the objective, we have selected 11 TPPO cocrystals<sup>13–23</sup> along with the TPPO.hemihydrate polymorphs to render the sample size and quality statistically acceptable (17 O–H...O interactions, Table 1) on the basis of the following factors: (i) varying geometrical attributes of the H-bonds (Table 2), (ii) different acidic H-bond donors, and (iii) inclusion of the covalent O–H...O interaction.

We have thoroughly examined the physical aspects of O–H...O interactions through four benchmark studies, viz., quantum theory of atoms in molecules (QTAIM),<sup>24,25</sup> intrinsic bond strength index (IBSI),<sup>26</sup> natural bond orbital (NBO),<sup>27,28</sup> and symmetry adapted perturbation theory (SAPT).<sup>29</sup> The computational results have truly insisted us for conducting statistically valid correlation analyses between the nonenergetic observables and H-bond interaction energy of versatile O–H...

O interactions. One such endearing nonenergetic structural parameter is the bond length ( $d_{\text{O–H...O}}$ ), but it fails to provide a direct quantification of the donor–acceptor interaction energy. From correlation analysis, we have herein propounded two avenues for a reliable and quick semiquantitative estimation of H-bond interaction energy from the H-bond length:  $d_{\text{O–H...O}} \rightarrow \rho_{\text{BCP}} \rightarrow E_{\text{SAPT0}}$  and  $d_{\text{O–H...O}} \rightarrow \text{IBSI} \rightarrow E_{\text{SAPT0}}$ . Such correlations can really foster a proclivity to use the easily accessible bond length values for gauging not only the existence of H-bonding in common parlance but also to probe the nature (closed-shell, intermediate, and covalent) and strength of the H-bonds as a frequent practice.

## 2. RESULTS AND DISCUSSION

**2.1. QTAIM Study.** QTAIM is an interpretative and quantitative approach to explore the nature of the intermolecular interactions in real space, since it affords (3, -1) critical points along the H...A bond paths (BPs) of the D-H...A intermolecular contacts. The relevant topological parameters of the TPPO.hemihydrate polymorphs and TPPO cocrystals at their concerned bond critical points (BCPs) have been collected in Table 1.

The electron density ( $\rho$ ) is one of the imperative quantum observables and  $\rho$  at the BCP, i.e.,  $\rho_{\text{BCP}}$ , can enlighten us regarding various aspects of chemical bonding to understand as well as to predict the properties of a molecule at the atomic level. The O-H...O interactions in the cocrystals consistently manifest higher  $\rho_{\text{BCP}}$  values along the H-bond paths compared to the TPPO.hemihydrate polymorphs. For the polymorphs, the  $\rho_{\text{BCP}}$  values are less than 0.025 au and with the progressive charge accumulation,  $\rho_{\text{BCP}}$  finally exceeds 0.1 au for the TPPO.nitric acid cocrystal. While the topological property of  $\rho(r)$  is chiefly governed by the dominance of the electron-nucleus force,<sup>30</sup> the topological property of its Laplacian,  $\nabla^2\rho(r)$ , emphasizes on the localization of electrons in space either to specify charge concentration or charge depletion.<sup>31,32</sup> At a BCP, when  $\nabla^2\rho(r) < 0$ , the electron density is locally concentrated and the depletion of local electron density is referred by the condition  $\nabla^2\rho(r) > 0$ .<sup>33</sup> Since, local electron density concentration indicates electron pair localization at any point, covalent contribution is considered to stabilize the concerned interaction. Barring the TPPO.nitric acid cocrystal, all the  $\nabla^2\rho_{\text{BCP}}$  values are positive in Table 1, and the noncovalent nature<sup>34,35</sup> has been attributed to the existential O-H...O interactions in the polymorphs and cocrystals except the TPPO.nitric acid.

Customarily, the magnitudes of both of the parameters, local electronic kinetic energy density  $G(r)$  and local electronic potential energy density  $V(r)$ , depend on the  $\rho_{\text{BCP}}$ . Therefore, a reduction in  $\rho_{\text{BCP}}$  should decrease the interelectronic repulsion, which consequently results in a depletion of the kinetic energy and also the potential energy. As a reliable measure to classify any hydrogen bonding interaction into closed-shell, intermediate and covalent types, the ratio of the two parameters, i.e., the  $|V(r)|/G(r)$  index, can be practically used.<sup>36</sup> Since all the observed O-H...O interactions in the polymorphs have been characterized by  $|V(r)|/G(r) < 1$ , those can be primarily regarded as the closed-shell interactions. For the cocrystals, the  $|V(r)|/G(r)$  parameter spans a wide range,  $2 < |V(r)|/G(r) < 1$ , and the O-H...O interactions appear really diverse from the perspective of bonding present therein.

We have felt an interest to scrutiny for handy correlations between the QTAIM topological descriptors and the bond lengths of the O-H...O interactions ( $d_{\text{O-H}\cdots\text{O}}$ ) in the structurally characterized cocrystals. To accomplish the purpose, the choice of the samples enlisted in Table 1 seems reasonable on the basis of the following factors: (i)  $\rho_{\text{BCP}}$  values span a wide window from 0.1044 to 0.0161 au, (ii) the lengths of O-H...O interactions cover a satisfactory range of 1.352–2.084 Å (Table 2), (iii) the angles of O-H...O interactions embrace a large domain of 143–177° (Table 2), and (iv) H-bond donors largely differ in their acidities. The correlation study is upper-bound at TPPO.nitric acid cocrystal (covalent), and the lowest limit has been marked by the TPPO.hemihydrate polymorphs (noncovalent).

At first, the quest for a correlation between the  $\rho_{\text{BCP}}$  and  $d_{\text{O-H}\cdots\text{O}}$  parameters seems sensible, as it can greatly facilitate the empirical calculation of  $\rho_{\text{BCP}}$  for practical use in any TPPO cocrystal. The correlation result is depicted in Figure 1, which

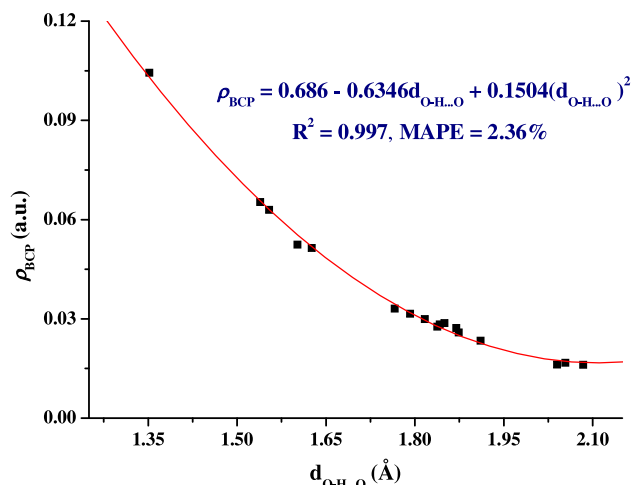


**Figure 1.** Second order polynomial relationship between the  $\rho_{\text{BCP}}$  values computed at M06-2X-D3/def2-TZVP level of theory (Table 1) and the crystallographically characterized O-H...O interaction distance (Table 2),  $d_{\text{O-H}\cdots\text{O}}$  (Å), for the TPPO.hemihydrate polymorphs and 11 other TPPO cocrystals.

reflects an excellent second order polynomial fit with a very high coefficient of determination value of 0.997. Being consistent with this magnificent fitting, the mean absolute percentage error (MAPE) has been reduced to only 2.36%. These accuracy parameters firmly suggest that the empirical equation,  $\rho_{\text{BCP}}$  (a.u.) =  $0.686 - 0.6346d_{\text{O-H}\cdots\text{O}}$  (Å) +  $0.1504(d_{\text{O-H}\cdots\text{O}})^2$  (Å<sup>2</sup>), is quite promising and conducive to calculate the  $\rho_{\text{BCP}}$  values quantitatively from the crystallographically determined O-H...O lengths. Since we have used the crystallographic atomic coordinates for the QTAIM computation, the empirical equation imbibes an average effect of various crystal packing patterns.

The covalent nature in the O-H...O interactions is regulated by the inherent stereoelectronic features of the H-bond donors and acceptors, and it cannot be easily predicted by a mere inspection. In this study, since the H-bond donors substantially differ from stereoelectronic viewpoint, we have rationally explored an empirical but effective way to trace the covalent character in the O-H...O interactions relying on the  $|V(r)|/G(r)$  value at the BCP, which discriminates among the closed-shell ( $|V(r)|/G(r) < 1$ ), intermediate ( $1 < |V(r)|/G(r) < 2$ ), and covalent ( $|V(r)|/G(r) > 2$ ) interactions.<sup>36</sup> A plot between the two parameters,  $|V(r)|/G(r)$  and  $d_{\text{O-H}\cdots\text{O}}$  has been portrayed in Figure 2, and the plot accords with a second order polynomial relation with a very good coefficient of determination ( $R^2 = 0.986$ ). Hence, the empirical equation,  $|V(r)|/G(r) = 11.150 - 10.0071d_{\text{O-H}\cdots\text{O}}$  (Å) +  $2.4088(d_{\text{O-H}\cdots\text{O}})^2$  (Å<sup>2</sup>), with a low MAPE of 2.83%, can serve as a very useful tool for a quick and reliable measure of the electronic nature of the O-H...O interactions in the structurally characterized cocrystals.

Therefore, two QTAIM parameters,  $\rho_{\text{BCP}}$  and  $|V(r)|/G(r)$ , consistently hold a general form of quadratic equation,  $y = ax^2 - bx + c$ , with the structural parameter  $d_{\text{O-H}\cdots\text{O}}$  and show parabolic curves. Both the leading coefficients ( $a$ ) are positive

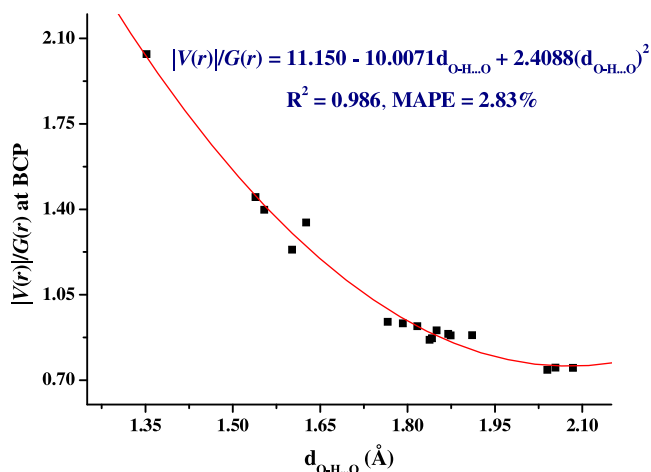


**Figure 2.** Polynomial regression plot between the  $|V(r)|/G(r)$  values and the crystallographically characterized O–H...O interaction distance,  $d_{\text{O–H}\cdots\text{O}}$  (Å), for the TPPO.hemihydrate polymorphs and 11 other TPPO cocrystals.

in the empirical equations, and the parabolas depicted in Figures 1 and 2 open upward. Since the value of  $a$  in Figure 2 is greater than that of Figure 1, it can be said that the parabola grows relatively faster between  $|V(r)|/G(r)$  and  $d_{\text{O–H}\cdots\text{O}}$  than in the case of  $\rho_{\text{BCP}}$  and  $d_{\text{O–H}\cdots\text{O}}$ .

**2.2. SAPT Analysis.** Energy decomposition analysis is the *sine qua non*, to explore various physically meaningful energy components associated with a noncovalent interaction, and the benchmark study in this aspect is the SAPT analysis.<sup>29</sup> In the domain of SAPT where many variants are available, the cardinal but effective form is SAPT0,<sup>37</sup> which performs best through favorable cancellation of errors and seems to be optimal with the truncated double- $\zeta$  basis set. Unless, rigorous precision is not the objective, the semiquantitative accuracy as obtained from the SAPT0 method is admissible for most applications to get an insightful description of electrostatic ( $E_{\text{elst}}$ ), exchange-repulsion ( $E_{\text{exch}}$ ), induction ( $E_{\text{ind}}$ ), and dispersion ( $E_{\text{dis}}$ ) energy components. Hence, the SAPT0 energy decomposition analysis using the aug-cc-pVDZ basis set can obviously enlighten us about the interaction energy and its components for the existential O–H...O interactions in the polymorphs and cocrystals.

From the  $E_{\text{SAPT0}}$  data collected in Table 2, it is evident that the relative stabilization of the intermolecular O–H...O interactions in the orthorhombic TPPO.hemihydrate is higher than the monoclinic varieties. For the polymorphs (lowest average  $E_{\text{SAPT0}}$  value), the electrostatic force contributes 67.3% on average, while the average contributions from the induction and dispersion forces are comparable, 15.3% and 17.4%, respectively. With the gradual increase in  $E_{\text{SAPT0}}$  value for the TPPO cocrystals, the contribution of induction energy progressively increases, and finally, it becomes almost equal to the electrostatic contribution in case of TPPO.nitric acid (45% electrostatics and 43% induction).

This notable revelation clearly suggests that the long-range electrostatic force makes a major contribution to the H-bond interaction energy for the weakly interacting polymorphs and cocrystals, while much less contribution stems from the induction energy. As shrinking in intermolecular separation starts (short H-bond distance), the electron clouds of the monomers approach closer to each other, creating a better possibility of overlap between their electron densities.

However, the Pauli exclusion principle prohibits the reinforcement of electrons of same spin in the nonbonded region. Consequently, the incompletely shielded positively charged nuclei mutually experience a repulsive force and that increases the magnitude of  $E_{\text{exch}}$  term.<sup>38</sup> In effect, cancellation between the electrostatic and exchange-repulsion energies becomes more conspicuous at smaller distances. For the TPPO.p-nitrophenol and TPPO.nitric acid cocrystals, the exchange-repulsion energy eventually becomes more positive than that of the electrostatic component. This acts as an impetus to the induction energy to enhance its contribution and eventually becomes almost the same as the electrostatic part for the TPPO.nitric acid cocrystal. Evidently, the set of polymorphs and TPPO cocrystals elegantly demonstrates a transformation of the glimmering role of induction into a dominant one with the reduction in O–H...O length. The variation of SAPT0 energy components with respect to the change in O–H...O length has been depicted in Figure 3 to gain an insight of the

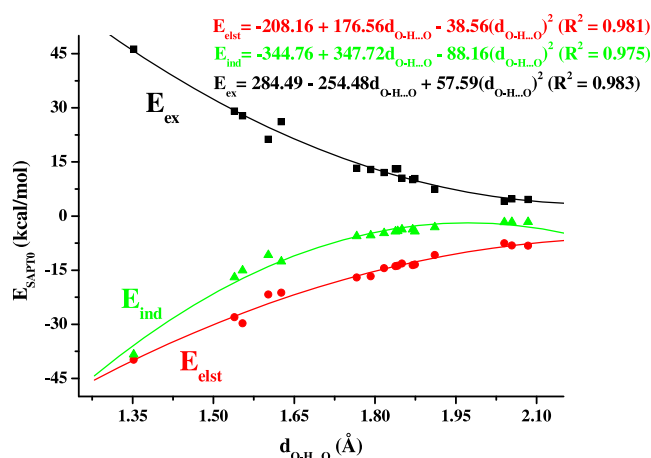


**Figure 3.** Variation of  $E_{\text{elst}}$ ,  $E_{\text{ind}}$ , and  $E_{\text{ex}}$  components with respect to  $d_{\text{O–H}\cdots\text{O}}$ , for the TPPO.hemihydrate polymorphs and other TPPO cocrystals.

impactful interplay among the  $E_{\text{elst}}$ ,  $E_{\text{ind}}$ , and  $E_{\text{ex}}$  components. Figure 3 also clarifies that the parabola grows relatively faster for the  $E_{\text{ind}}$  compared to the  $E_{\text{elst}}$  and  $E_{\text{ex}}$  components, i.e., the variation of  $E_{\text{ind}}$  is mostly sensitive to the change in  $d_{\text{O–H}\cdots\text{O}}$  for the TPPO cocrystals.

It now seems rational to investigate the variation of four SAPT0 energy components with respect to interaction energies of the O–H...O interactions that span a wide energy range from  $-7$  to  $-42$  kcal/mol (Table 2). The interrelationship results have been depicted in Figure 4, which reflects that the four fundamental SAPT0 energy terms bear satisfactory linear relationship with the O–H...O interaction energies. We have intentionally omitted four prominent outliers only around the  $E_{\text{dis}}$  regression line for the TPPO cocrystals of nitric acid, diphenylmethanol, trimethylphenylboronic acid, and 6-chloro-2-pyridinol, which would otherwise cause a drop of  $R^2$  to an unacceptable value near 0.50. The  $E_{\text{ind}}$  and  $E_{\text{dis}}$  lines are converging in nature, and  $E_{\text{dis}}$  is more contributing than  $E_{\text{ind}}$  to  $E_{\text{SAPT0}}$  when the strength of the O–H...O interaction is less than  $-12.5$  kcal/mol particularly for the polymorphs. With the increase in strength of the O–H...O bonds beyond  $-12.5$  kcal/mol, the  $E_{\text{ind}}$  line intersects the  $E_{\text{dis}}$  line due to 2.5 times steeper slope and becomes more contributing. As the  $E_{\text{elst}}$  and  $E_{\text{ind}}$  lines are approaching almost parallel to each other and

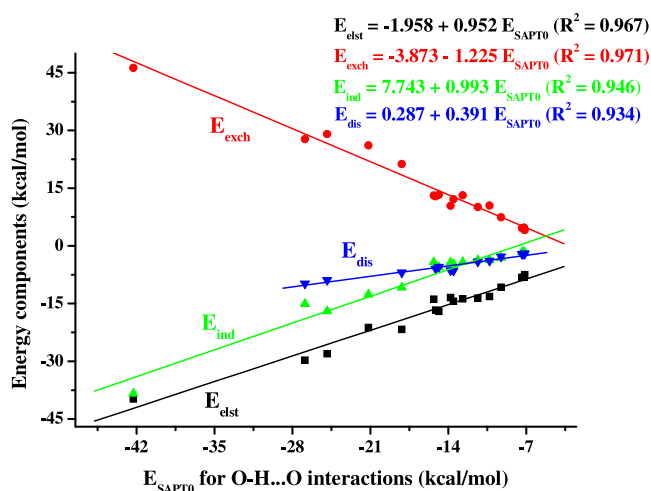


**Figure 4.** Variation of four SAPTO energy components with respect to the O–H...O interaction energy for the polymorphs and TPPO cocrystals.

dipping steadily at higher  $E_{\text{SAPTO}}$  values, both terms effectively control the magnitude of  $E_{\text{SAPTO}}$ . An appreciably linear correlation ( $R^2 = 0.967$ ) between the  $E_{\text{elst}}$  and  $E_{\text{SAPTO}}$  terms with an acceptable MAPE value of 7.75% has led us to believe that a semiquantitative estimate of the electrostatic component in H-bond interactions can be conveniently extracted from the expression  $E_{\text{elst}}$  (kcal/mol) =  $-1.958 + 0.952E_{\text{SAPTO}}$  (kcal/mol). The MAPEs for the other energy components lie within a tolerable range of 8–11% and those also seem to be fit for use in TPPO cocrystals.

One intriguing aspect that still remains unexamined is the impact of a QTAIM-based fundamental property,  $\rho_{\text{BCP}}$ , on  $E_{\text{SAPTO}}$  of the O–H...O interactions. The  $\rho_{\text{BCP}}$  values of the entire data set comprising of 17 O–H...O interactions have been collected in Table 1, and the  $E_{\text{SAPTO}}$  values are given in Table 2. The regression plot of  $E_{\text{SAPTO}}$  against  $\rho_{\text{BCP}}$  has been showcased in Figure 5. The correlation fits with a linear equation,  $E_{\text{SAPTO}}$  (kcal/mol) =  $-381.28\rho_{\text{BCP}}$  (a.u.)  $- 1.578$ , which exhibits a satisfying  $R^2$  value of 0.966 and a tolerable MAPE of 9.26%. Therefore, this relation can be employed for a

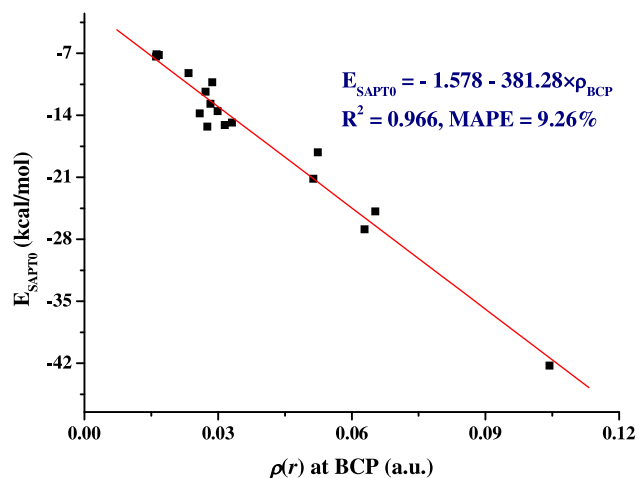


**Figure 5.** Linear regression plot of the total interaction energy ( $E_{\text{SAPTO}}$ ) against the  $\rho_{\text{BCP}}$  for the O–H...O interactions in the polymorphs and cocrystals.

fast calculation of the O–H...O interaction energy at the SAPTO level for semiquantitative purposes pertinent to the other TPPO cocrystals.

At this point, it seems instructive to check the relative efficacy of three well acclaimed empirical equations: (i)  $E_{\text{HB}}^1$  (kcal/mol) =  $627.5V(r)/2$  proposed by Espinosa et al.,<sup>39</sup> (ii)  $E_{\text{HB}}^2$  (kcal/mol) =  $-223.08\rho(r) + 0.7423$  proposed by Emamian et al.<sup>40</sup> for the neutral complexes, and (iii)  $E_{\text{HB}}^3$  (kcal/mol) =  $-332.34\rho(r) - 1.0661$  proposed by Emamian et al.<sup>40</sup> for the charged species, to forecast the interaction energy for the polymorphs and cocrystals. All of the empirical values of interaction energy have been given in Table S19. The  $E_{\text{HB}}^1$  empirical values are uniformly lower at a moderate extent than their respective  $E_{\text{SAPTO}}$  counterparts, and the underestimated values show a 30–50% deviation from the SAPTO energies particularly for the TPPO.hemihydrate polymorphs. However, Emamian's empirical equation,  $E_{\text{HB}}^3$  (kcal/mol) =  $-332.34\rho(r) - 1.0661$ , has yielded improved  $E_{\text{HB}}^3$  values that manifest an average deviation of 8.7% with respect to the  $E_{\text{SAPTO}}$  values for the polymorphs. Using our empirical relation,  $E_{\text{HB}}^4$  (kcal/mol) =  $-381.28\rho_{\text{BCP}}$  (a.u.)  $- 1.578$ , an average deviation of 9.3% has been noted for the polymorphs, which suggests a comparable efficacy of the two equations ( $E_{\text{HB}}^3$  and  $E_{\text{HB}}^4$ ) at the limit of weak H-bonding. However, the  $E_{\text{HB}}^3$  values for 11 TPPO cocrystals of moderate to strong H-bond donors register 16.4% average deviation in contrast to 9.2% as observed with our empirical formula (Table S19). Therefore, Emamian's  $E_{\text{HB}}^3$  values for the TPPO cocrystals do not meet up to the expectations due to two reasons: (i) sampling of the charged species did not include the very electronic nature of the phosphoryl oxygen atom as the H-bond acceptor and (ii) crystal-specific local stereoelectronic effects remain unaccounted. Furthermore, Espinosa's  $E_{\text{HB}}^1$  and Emamian's  $E_{\text{HB}}^3$  empirical values are much comparable when the electron density at the BCP along the H-bond path is on a higher side ( $>0.05$  au), and either one of the two cannot be prioritized. As a general observation, the  $E_{\text{HB}}^2$  empirical values (Table S19) fail miserably to cope with the SAPTO energies of the polymorphs and TPPO cocrystals.

The lackluster performance of the empirical equation proposed for the neutral species,  $E_{\text{HB}}^2$  (kcal/mol) =  $-223.08\rho(r) + 0.7423$ , is extremely significant and implicative in the context of ascertaining the electronic nature of the phosphoryl group. A complete collapse of the above equation in this study led us to assume that the phosphoryl moiety present in the polymorphs and the cocrystals is not just a prototypical P=O fragment. Instead, the phosphoryl oxygen atom in the lattice may experience substantially higher negative charge than what is expected from the usual dipolar phosphoryl group. This issue has been duly investigated in the NBO analysis section.

**2.3. Better QTAIM Index for Covalency:  $IV(r)/G(r)$  or  $H(r)/\rho(r)$ ?** Mulliken and Person<sup>41</sup> had pioneered the concept of covalency in the form of intermolecular charge transfer occurring from the HOMO of the donor to the LUMO of the acceptor moieties, which in turn triggers charge reorganization in the two monomers of any adduct. This fact has prompted us to investigate the issue of charge transfer in the O–H...O interactions through the correlation study between the SAPT-derived induction energy and QTAIM topological descriptors. Two QTAIM descriptors, viz.,  $IV(r)/G(r)$  and  $H(r)/\rho(r)$  at BCP, have been proclaimed to assess the covalent character in H-bonds.<sup>36</sup> The condition of covalency, if assigned by the I

$V(r)/G(r)$  index, has been mentioned in the QTAIM section and the  $H(r)/\rho(r)$  parameter, known as the “bond degree”, distinguishes between the covalent and noncovalent H-bond interactions merely by its sign. A negative value of  $H(r)/\rho(r)$  at BCP is referred to a covalent interaction and positive value points for a noncovalent interaction. Although the charge transfer energy has not been categorically dealt with by the SAPT, it is an inclusive component of the SAPT-derived induction energy. Therefore, correlation analyses between  $|V(r)/G(r)|$  and  $E_{\text{ind}}$  as well as  $H(r)/\rho(r)$  and  $E_{\text{ind}}$  are indeed instructive to gauge the extent of covalent character in the H-bond interactions.

The plot depicted in Figure 6 between  $E_{\text{ind}}$  and  $|V(r)/G(r)|$  exhibits a second order polynomial regression with an excellent

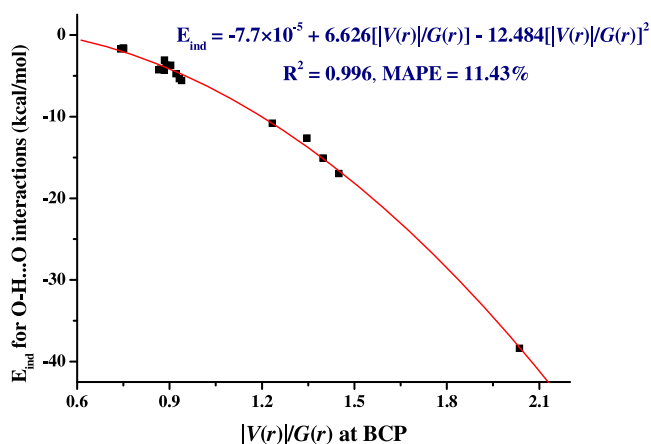


**Figure 6.** Quadratic regression plot of the SAPT-derived  $E_{\text{ind}}$  component against the  $|V(r)/G(r)|$  at BCP for the O–H...O interactions in the polymorphs and cocrystals.

coefficient of determination,  $R^2 = 0.996$ . However, the empirical dependence,  $E_{\text{ind}}$  (kcal/mol) =  $6.626|V(r)/G(r) - 12.484[|V(r)/G(r)]^2$  manifests a relatively higher MAPE of 11.43%. It is quite interesting to note that, for the five TPPO cocrystals of nitric acid, p-nitrophenol, 3,5-dinitrobenzoic acid, 1-naphthoic acid, and diphenylmethanol having  $|V(r)/G(r)$  value greater than unity (Table 1), the MAPE has been drastically reduced to 2.56%, whereas the MAPE has risen to 15.12% for the rest of the 12 O–H...O interactions having  $|V(r)/G(r)$  value less than unity. The above trend of MAPE implies that the H-bond interactions with  $|V(r)/G(r)| > 1.2$  respond in a well behaved manner to the change in  $E_{\text{ind}}$ , and the aspect of covalency can be a pertinent issue to search for. Scattering has been discerned for the H-bond interactions with  $|V(r)/G(r)| < 1$ , and the  $E_{\text{ind}}$  cannot provide a trustworthy roadmap for ascertaining the covalent character in the H-bonds since charge transfer is paltry in those interactions.

The empirical dependence of  $E_{\text{ind}}$  on  $H(r)/\rho(r)$  is again second order polynomial in nature with a  $R^2$  value of 0.973 (Figure 7). Despite having an acceptable coefficient of determination, the data points are quite spread out around the fitted line, which makes an enormous MAPE of 33.19%. Even for the five well-behaved cocrystals in Figure 6, the MAPE in this case has reached to 9.58% and the MAPE for the remaining 12 O–H...O interactions escalates to a staggering 43.03%. This observation clearly reflects that the relation  $E_{\text{ind}}$  (kcal/mol) =  $-4.789 + 20.269[H(r)/\rho(r)] - 59.034[H(r)/$

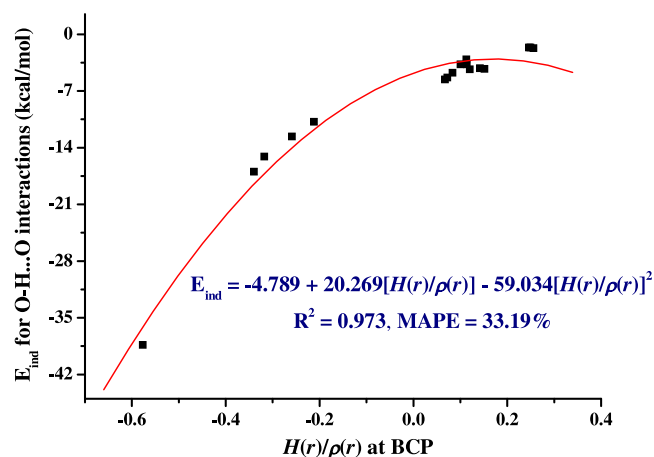


**Figure 7.** Quadratic regression plot of the SAPT-derived  $E_{\text{ind}}$  component against the  $H(r)/\rho(r)$  at BCP for the O–H...O interactions in the polymorphs and cocrystals.

$\rho(r)]^2$  fails to forecast the  $E_{\text{ind}}$  value for any of the O–H...O bonds.

By analyzing the accuracy parameters of the two plots given in Figures 6 and 7, we can safely conclude that the QTAIM descriptor  $|V(r)/G(r)|$  has to be primarily chosen over the  $H(r)/\rho(r)$  parameter to predict the  $E_{\text{ind}}$  value as a testament of covalent character in the O–H...O interactions.

**2.4. NBO Analysis.** From the preceding SAPT0 analysis, it has been affirmed that the TPPO.nitric acid cocrystal represents the strongest O–H...O hydrogen bonding, and the TPPO.hemihydrate polymorphs exhibit the weakest. Therefore, the NBO analysis (at the M06-2X-D3/def2-TZVP level) for these two systems of opposite extremes can guide us to understand the facets of hydrogen bonding with regard to (i) the electronic nature of the phosphoryl moiety which remains H-bonded with various donors and (ii) the influence of charge transfer phenomenon in stabilizing the intermolecular O–H...O interactions.

Let us begin with a pertinent discussion on the change in energy and orbital composition of the phosphoryl lone pairs against the variation of the H-bond donors. The gist has been highlighted in Figure 8. It has been uniformly observed from the NBO analysis that the oxygen atom of the phosphoryl motif houses three lone pairs ( $n_{1O}$ ,  $n_{2O}$ , and  $n_{3O}$ ) in the polymorphs and cocrystals. For the polymorphs, two of them ( $n_{2O}$  and  $n_{3O}$ ) are degenerate (energy difference  $< 1$  kcal/mol) and made up of an almost exclusive p-character ( $> 99.5\%$ ). The other lone pair ( $n_{1O}$ ) exhibits an admixture of 60% s- and 40% p-character. Therefore, the phosphoryl-oxygen based lone pairs show 2 + 1 degeneracy in the polymorphs. In the TPPO.3,5-dinitrobenzoic acid cocrystal, the  $n_{3O}$  lone pair has just started to accumulate s-character (3%), and the  $n_{2O}$  and  $n_{3O}$  lone pairs have been separated by 18 kcal/mol. In effect, the degeneracy of the  $n_{2O}$  and  $n_{3O}$  lone pairs is lifted, and three lone pairs form 1 + 1 + 1 degenerate sets due to s-p orbital mixing. The infusion of s-character in the  $n_{3O}$  lone pair has reached maximum in TPPO.nitric acid, and the  $n_{2O}$  and  $n_{3O}$  lone pairs are now separated by 101 kcal/mol. In fact, three lone pairs of the phosphoryl oxygen atom in TPPO.nitric acid cocrystal have become completely nonequivalent in terms of orbital composition ( $n_{1O}$ : 40% s + 60% p,  $n_{2O}$ :  $> 99.5\%$  p,  $n_{3O}$ : 22% s + 78% p).

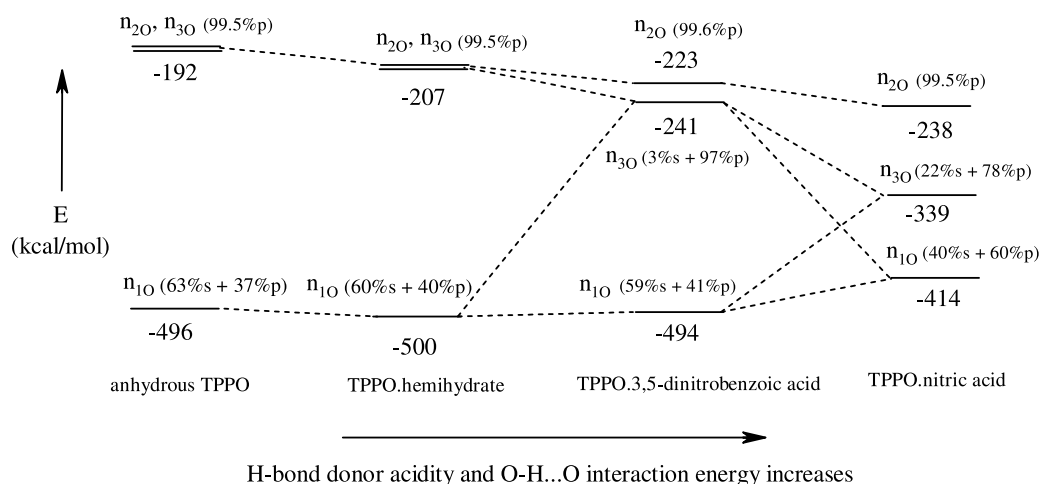


**Figure 8.** Depiction of change in energy (not to scale) and orbital composition in the phosphoryl lone pairs on going from anhydrous TPPO to TPPO.hemihydrate followed by TPPO.3,5-dinitrobenzoic acid and finally to TPPO.nitric acid.

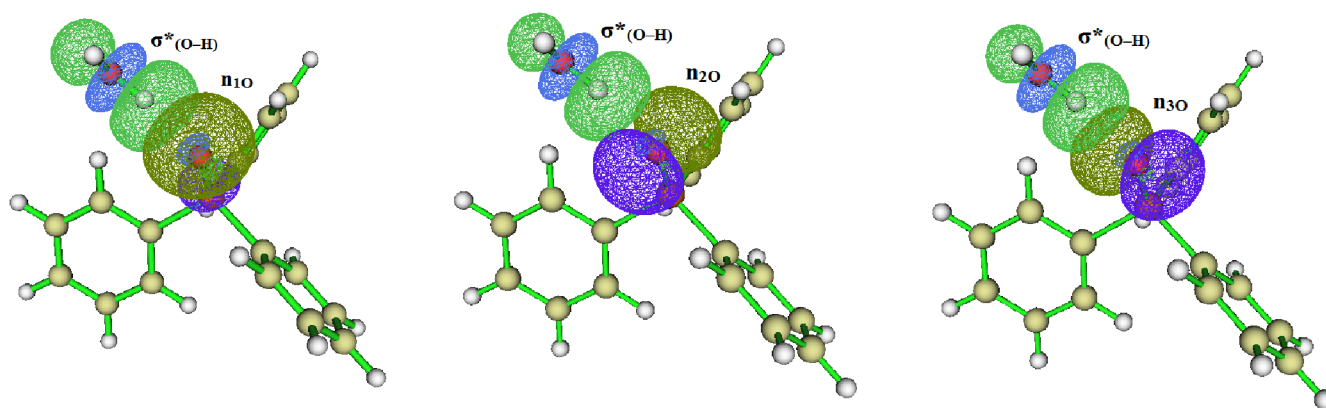


**Figure 9.** Orbital orientations for all three theoretically possible  $n_{10} \rightarrow \sigma^*_{(O-H)}$  charge transfer pathways in the case of orthorhombic TPPO.hemihydrate polymorph.

A concomitant reshuffling of energy is obvious as a consequence of this gradual change in the orbital composition of the lone pairs. The energy of  $n_{20}$  slowly declines with the increase in H-bond strength since the gross p-orbital character is retained all-through. The energy of  $n_{30}$  reduces faster due to progressive incorporation of s-character from the  $n_{10}$  lone pair. Oppositely, the energy of the  $n_{10}$  lone pair moderately enhances due to the loss of s-character with the increase in H-bond strength. The energy gap between the highest-energy and lowest-energy lone pairs depletes through the sequence, anhydrous TPPO<sup>42</sup> (304 kcal/mol)  $\rightarrow$  TPPO.hemihydrate (293 kcal/mol)  $\rightarrow$  TPPO.3,5-dinitrobenzoic acid (271 kcal/mol)  $\rightarrow$  TPPO.nitric acid (176 kcal/mol). Therefore, we can infer that an enhancement of proton releasing ability of the H-bond donors induces more polarization to the phosphoryl lone pairs and electron density reinforcement happens along the H-bond path.

To clarify the first issue regarding the electronic nature of the H-bonded phosphoryl group, second order perturbation theory analysis has been carried out, and the results demonstrate that three types of intramolecular charge transfer pathways can be theoretically operative for every single TPPO.hemihydrate polymorph:  $n_{20}, n_{30} \rightarrow 3d(P)$ ,  $n_{10} \rightarrow$  Rydberg sp hybrid(P), and  $n_{20}, n_{30} \rightarrow \sigma^*_{P-C_{ipso}}$ . The energy differences between the acceptor and donor levels for the  $n_{20}, n_{30} \rightarrow \sigma^*_{P-C_{ipso}}$  and  $n_{20}, n_{30} \rightarrow 3d(P)$  charge transfer

pathways are ca. 400 and ca. 950 kcal/mol, respectively. Surpassing such energy barriers, charge transfer, if it occurs, only affords ca. 40 kcal/mol and ca. 10 kcal/mol interaction energy for the  $n_{20}, n_{30} \rightarrow \sigma^*_{P-C_{ipso}}$  and  $n_{20}, n_{30} \rightarrow 3d(P)$  paths, respectively. On the other hand, the  $n_{10} \rightarrow$  Rydberg sp hybrid(P) charge transfer has been computed to occur across a huge energy gap of ca. 1400 kcal/mol to impart an insignificant interaction energy of ca. 10 kcal/mol. Apparently, the computed energy differences involving the “non-Lewis valence 3d” and “extra-valence Rydberg” acceptor orbitals are almost realistically unsurpassable at the ground state and consequently overrule any real significance of the phosphorus-based 3d-orbital participation in the bonding of the phosphoryl moiety. Without any noticeable change, a very similar energy trend has been observed for the intramolecular charge transfers in the cocrystals, and the previous conclusion sustains unambiguously.

All the above revelations strongly emphasize on an overwhelming contribution of the Lewis-compatible phosphoryl motif ( $\sigma_{P-O} = 0.5056(sp^{2.56}d^{0.04})_P + 0.8628(sp^{1.51})_O$ ,  $\sigma_{P-O} = 0.5063(sp^{2.54}d^{0.04})_P + 0.8624(sp^{1.52})_O$ ,  $\sigma_{P-O} = 0.5066(sp^{2.56}d^{0.04})_P + 0.8622(sp^{1.54})_O$  for *Fdd2*, *C2/c* and *Cc* polymorphs, respectively) in the ground state of the TPPO.hemihydrate polymorphs and also for the TPPO.nitric acid cocrystal ( $\sigma_{P-O} = 0.4945(sp^{2.80}d^{0.05})_P + 0.8692(sp^{1.62})_O$ ). Since, the Lewis-type electron count exceeds 97% of the total

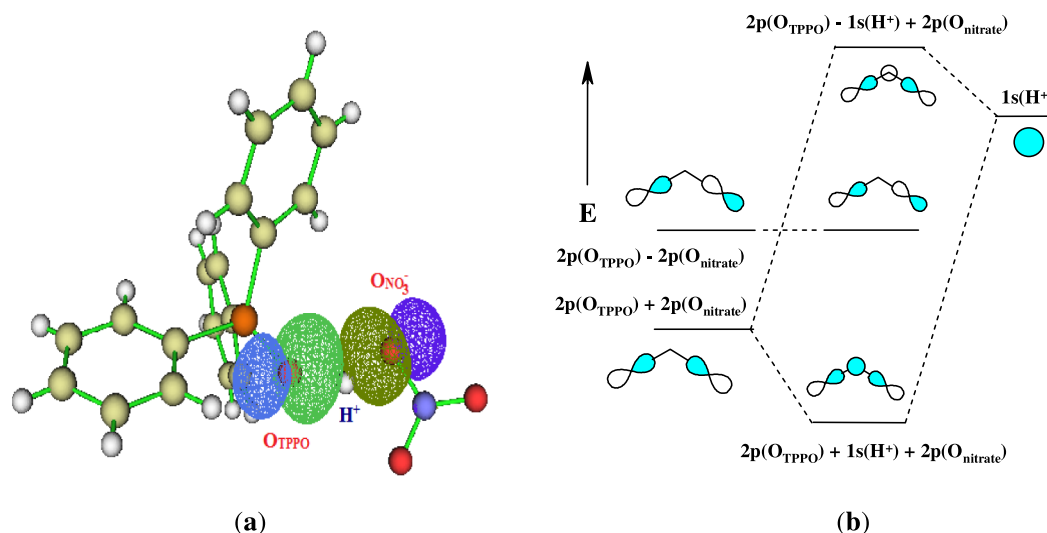


**Figure 10.** (a) Orbital orientations for the concurrent  $\text{O}_2\text{N}-\text{O}^- \rightarrow \text{H}^+$  and  $\text{Ph}_3\text{P}^+-\text{O}^- \rightarrow \text{H}^+$  charge transfer paths in the TPPO.nitric acid cocrystal at the M06-2X-D3/def2-TZVP level of theory. (b) Qualitative 3c-4e orbital interaction diagram for the  $\text{O}-\text{H}\cdots\text{O}$  interaction in the TPPO.nitric acid.

electrons for the TPPO motif in each of the polymorphs and cocrystals, a zwitterionic form  $\text{Ph}_3\text{P}^+-\text{O}^-$  has been proclaimed under the purview of NBO study instead of adhering to a prototypical  $\text{P}=\text{O}$  fragment.

To address the second issue regarding the charge transfer contribution to the intermolecular  $\text{O}-\text{H}\cdots\text{O}$  interactions, we have scrutinized all the three possible modes of  $n_{\text{O}} \rightarrow \sigma^*_{\text{O}-\text{H}}(\text{H}_2\text{O})$  orbital interactions (Figure 9) for the TPPO-hemihydrate polymorphs. Energy differences between the acceptor ( $\sigma^*_{\text{O}-\text{H}}$ ) and the donor ( $n_{1\text{O}}$ ) levels for the  $n_{1\text{O}} \rightarrow \sigma^*_{\text{O}-\text{H}}(\text{H}_2\text{O})$  path fall in the range of 845–850 kcal/mol, and their corresponding interaction energies span a range of only 2.8–5.2 kcal/mol in the crystal polymorphs. The remaining degenerate intermolecular charge transfer routes,  $n_{2\text{O}} \rightarrow \sigma^*_{\text{O}-\text{H}}(\text{H}_2\text{O})$  and  $n_{3\text{O}} \rightarrow \sigma^*_{\text{O}-\text{H}}(\text{H}_2\text{O})$ , exist across the energy gap of 545–555 kcal/mol to impart a meager 0.1–2.75 kcal/mol interaction energy. Since the energy difference between any one of the donor orbitals ( $n_{1\text{O}}$ ,  $n_{2\text{O}}$ , and  $n_{3\text{O}}$ ) of TPPO and the fixed acceptor orbital ( $\sigma^*_{\text{O}-\text{H}}$ ) of lattice water is just massive to yield a very small interaction energy, a physically meaningful charge transfer component in the  $\text{O}-\text{H}\cdots\text{O}$  interaction cannot be asserted. The impression has been rightly attested to from a very low average electron density (0.011e) in the  $\sigma^*_{\text{O}-\text{H}}(\text{H}_2\text{O})$  orbital of lattice water for the polymorphs.

The scenario radically changes in the TPPO.nitric acid cocrystal, where the formally vacant H-centered valence non-Lewis orbital (chemically equivalent to 1s orbital of  $\text{H}^+$ ) shows a population of 0.441e. Since NBO study shows that the TPPO.nitric acid lattice is composed of three fragments (TPPO, H, and  $\text{NO}_3$ ), the proton is obviously under the dual control of TPPO and nitrate groups. Second order perturbation theory analysis has unfolded two viable charge transfer pathways:  $\text{O}_2\text{N}-\text{O}^- \rightarrow \text{H}^+$  and  $\text{Ph}_3\text{P}^+-\text{O}^- \rightarrow \text{H}^+$  (Figure 10a). The charge transfer energy in the former route is 200.2 and 122.0 kcal/mol through the latter route. Without any ambiguity, the results indicate that the flanked H atom is interacting sufficiently with both the TPPO and nitrate motifs, and appreciable covalency has been incorporated in the  $\text{O}-\text{H}\cdots\text{O}$  interaction. In the issue of covalency, a very high  $|\nabla(r)|/$

$G(r)$  value exceeding 2.0 as well as a negative  $\nabla^2\rho(r)$  value for the  $\text{O}-\text{H}\cdots\text{O}$  interaction in TPPO.nitric acid cocrystal (QTAIM analysis, vide Table 1) corroborate the NBO results. From X-ray diffraction study,<sup>19</sup> it has been authenticated that the  $\text{O}_{(\text{TPPO})}\cdots\text{H}^+$  and  $\text{O}_{(\text{nitrate})}\cdots\text{H}^+$  distances, 1.352 and 1.303 Å respectively, do not largely differ and the  $\text{O}_{(\text{TPPO})}\cdots\text{H}^+\cdots\text{O}_{(\text{nitrate})}$  contact is bent ( $143^\circ$ ). As suggested by the Mayer bond orders: 0.29 for  $\text{O}_{(\text{TPPO})}\cdots\text{H}^+$  and 0.50 for  $\text{O}_{(\text{nitrate})}\cdots\text{H}^+$  interactions, a moderately strong 3c-4e bonding can be invoked to model the electron delocalization occurring in the bent  $\text{O}_{(\text{TPPO})}\cdots\text{H}^+\cdots\text{O}_{(\text{nitrate})}$  motif. The relevant orbital interaction diagram is given in Figure 10b. No such 3c-4e bonding model can be extended to the TPPO.hemihydrate polymorphs despite of having much linear  $\text{O}-\text{H}\cdots\text{O}$  bonds ( $\angle\text{O}-\text{H}\cdots\text{O} > 170^\circ$ ).

The glimmering role of charge transfer in linear  $\text{O}-\text{H}\cdots\text{O}$  interactions of the polymorphs and a dominant role of charge transfer in the TPPO.nitric acid cocrystal as revealed by SAPT analysis are in congruence with the NBO results. The explicitly conveyed facts by the NBO analysis are (i) the weak  $\text{O}-\text{H}\cdots\text{O}$  hydrogen bonds should be described as the charge-assisted  $\text{Ph}_3\text{P}^+-\text{O}^-\cdots\text{H}^{\delta+}-\text{O}^{\delta-}-\text{H}$  interaction instead of  $\text{Ph}_3\text{P}^{\delta+}=\text{O}^{\delta-}\cdots\text{H}^{\delta+}-\text{O}^{\delta-}-\text{H}$  type dipolar attraction, while the very strong  $\text{O}-\text{H}\cdots\text{O}$  bonds can be mapped by the 3c-4e delocalized bonding, (ii) there exists a broad perspective of bonding within which any other TPPO.H-bond donor cocrystal of intermediate H-bond strength can fit in its own place, and (iii) the putative idea of enhanced charge transfer with the increase in orbital directionality does not succeed for the polymorphs and TPPO.nitric acid cocrystal, instead the properties like compatibility in symmetry and energy of the orbitals are decisive.

**2.5. IBSI Analysis.** Recently developed intrinsic bond strength index (IBSI)<sup>26</sup> concept has been emerged from the independent gradient model (IGM)<sup>43,44</sup> and diverges from other orthodox bond orders (Mulliken,<sup>45</sup> Wiberg<sup>46</sup> or Mayer)<sup>47,48</sup> in the sense that IBSI depends on local stretching bond force constant between the two selected atoms in any molecular environment. IBSI is a dimensionless value, which can estimate the nature of chemical bonds and quantitatively

**Table 3.** Collection of the O–H···O Lengths, their Inverse Square Values,  $E_{\text{SAPT0}}$  Values along with the Magnitudes of IBSI Computed at M06-2X-D3/def2-TZVP Level of Theory<sup>a</sup>

cocrystals and polymorphs	O–H···O distance ( $d$ , Å)	$d^{-2}$ (Å <sup>-2</sup> )	IBSI	$E_{\text{SAPT0}}$ (kcal/mol)
TPPO.nitric acid	1.352	0.547	0.3224	-42.28
TPPO.p-nitrophenol	1.539	0.422	0.1338	-24.87
TPPO.3,5-dinitrobenzoic acid	1.554	0.414	0.1234	-26.87
TPPO.1-naphthoic acid	1.602	0.389	0.0999	-18.18
TPPO.dephenylmethanol	1.626	0.378	0.1044	-21.17
TPPO.3-chlorobenzoic acid	1.766	0.321	0.0577	-14.84
TPPO.pentafluorophenol	1.792	0.311	0.0563	-15.12
TPPO.hydroquinone	1.817	0.303	0.0533	-13.53
TPPO.trimethylphenylboronic acid	1.838	0.296	0.0485	-15.29
TPPO.6-chloro-2-pyridinol	1.842	0.294	0.0495	-12.71
TPPO.hydrogenperoxide	1.850	0.292	0.0481	-10.29
TPPO.hydrogenperoxide	1.870	0.286	0.0467	-11.35
TPPO.hydroquinone	1.874	0.284	0.0466	-13.79
TPPO.hemihydrate ( <i>Fdd2</i> )	1.911	0.274	0.0417	-9.25
TPPO.hemihydrate ( <i>C2/c</i> )	2.040	0.240	0.0279	-7.13
TPPO.hemihydrate ( <i>Cc</i> )	2.054	0.237	0.0284	-7.19
TPPO.hemihydrate ( <i>Cc</i> )	2.084	0.230	0.0262	-7.37

<sup>a</sup> $E_{\text{SAPT0}}$  values have been computed using the aug-cc-pVDZ basis set.

distinguish covalent ( $4.0 > \text{IBSI} > 0.15$ ) from noncovalent interactions ( $0 < \text{IBSI} < 0.15$ ). Since IBSI provides a measure of bond strength and has not been anywhere explored previously in the context of H-bonding involving the phosphoryl motif, we have felt the urge to apply IBSI analysis for the O–H···O bonds in all the cocrystals and polymorphs (Table 3) to evaluate their intrinsic nature and strength. An inspection of the IBSI values clearly reveals that barring the covalent O–H···O interaction in TPPO.nitric acid cocrystal, all other interactions are noncovalent in nature.

Since it is not unrealistic to assume that H-bond interaction energy should have a dependence on the force constant of a growing bond between the donor and the acceptor atoms, we have examined the relationship between the  $E_{\text{SAPT0}}$  interaction energies and IBSI values for a diverse set of closed-shell and covalent H-bond interactions given in Table 3. Two relevant parameters correlate satisfactorily through a quadratic equation,  $E_{\text{SAPT0}}$  (kcal/mol) =  $-2.383 - 214.87(\text{IBSI}) + 283.39(\text{IBSI})^2$ , with  $R^2 = 0.968$ , and the corresponding parabolic curve has been given in Figure 11. From a high  $R^2$  value, it seems that  $E_{\text{SAPT0}}$  is fairly connected with IBSI. However, some extent of scattering of the data points around the fitted curve has been observed. This may happen for the O–H···O bonds which are considerably electrostatic in origin and therefore exhibit low stretching force constant especially in the lower IBSI region. Sporadic departures at relatively higher IBSI values may arise from specific lattice packing. Fortunately, the quadratic equation leads to an acceptable MAPE value of 9.66% and deems fit to calculate the empirical  $E_{\text{SAPT0}}$  values for semiquantitative purposes. Although the H-bond interaction energies have not been computed at the gold-standard level, this semiquantitative accuracy is acceptable for many applications that do not demand rigorous precision.

Now, with the help of the above empirical equation, we can set an energy scale (Figure 12) to probe the nature of any O–H···O interaction in the TPPO cocrystals. As per prescribed IBSI limit for noncovalent interactions ( $0 < \text{IBSI} < 0.15$ ),<sup>26</sup> when the O–H···O interaction energy lies within the range  $-2.5$  to  $-31.0$  kcal/mol, the respective interaction can be considered as noncovalent, in which electrostatic, induction,

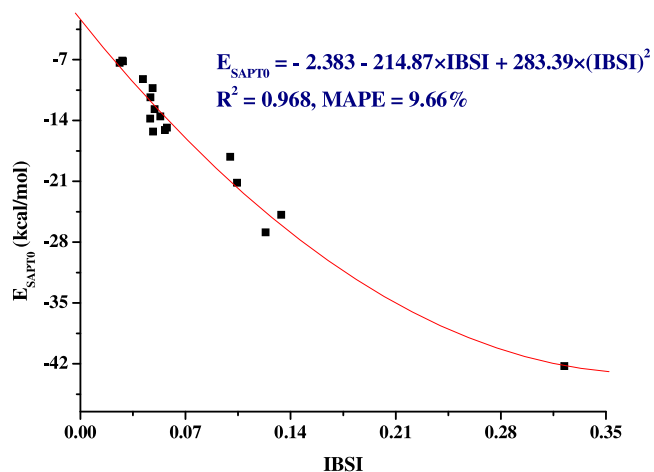


**Figure 11.** Quadratic regression curve correlating  $E_{\text{SAPT0}}$  and IBSI indices for the O–H···O interactions in TPPO cocrystals and polymorphs.



**Figure 12.** Proposed O–H···O interaction energy scale (SAPT0/aug-cc-pVDZ) in TPPO cocrystals based on the analysis of the IBSI parameter. Energy limits are indicative for the 17 H-bonds analyzed here.

and dispersion forces contribute to a varying extent. Beyond the upper limit, the interaction gradually advances into the covalent type (charge transfer), and below the lower limit, the interaction transitions into the van der Waals/dispersion type.

As IBSI is known to depend on the internuclear distance, it seems worthy to find its dependence on the crystallographically characterized O–H···O lengths. Through a quadratic regression, IBSI values have been satisfactorily correlated with the inverse square of the O–H···O interaction lengths (Table 3, Figure 13). The corresponding equation of the second order polynomial fit,  $\text{IBSI} = 0.1652 - 1.203d_{\text{O-H}\cdots\text{O}}^{-2}$  (Å<sup>-2</sup>) +

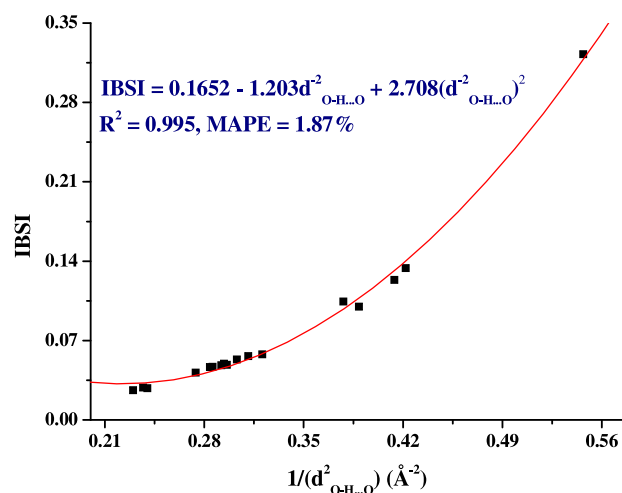


**Figure 13.** Quadratic regression plot between the IBSI and  $1/d^2_{\text{O-H}\cdots\text{O}}$  indices for the O-H $\cdots$ O interactions in the TPPO cocrystals and polymorphs.

$2.708(d^2_{\text{O-H}\cdots\text{O}})^2 (\text{\AA}^{-4})$ , has an excellent coefficient of determination of 0.995 and a very low MAPE of 1.87%. Therefore, this expression can be used to quantitatively predict the IBSI with optimum accuracy while the crystallographic O-H $\cdots$ O distance is known. Expectedly, IBSI increases with a decrease in the O-H $\cdots$ O length. Based on the IBSI values, the H-bond donors can be categorized in order of their potential: mineral acid > aromatic carboxylic acid > aromatic alcohol > aromatic diol > hydrogen peroxide > water. The order as evolved from this study is indicative, and it may disagree under the influence of any unaccounted crystal-specific packing force (solid state effect).

### 3. CONCLUSION

Through an extensive comparative analysis of the polymorphs and the 11 TPPO cocrystals, we want to enumerate the following findings as the conclusions.

(i) As a salient structural feature, the TPPO.hemihydrate polymorphs and all of the cocrystals uniformly exhibit the  $\text{Ph}_3\text{P}^+-\text{O}^-$  zwitterionic form in their ground states. Three oxygen-based lone pairs in the polymorphs split into 2 + 1 degenerate levels enriched in p-character and sp-character, respectively. 2-fold degenerate lone pairs further split into 1 + 1 degenerate levels with the increase in the H-bond strength for the cocrystals, rendering the three lone pairs nonequivalent with respect to energy and orbital composition.

(ii) From the QTAIM study, we have propounded two well-tolerated empirical relationships,  $\rho_{\text{BCP}} (\text{a.u.}) = 0.686 - 0.6346d_{\text{O-H}\cdots\text{O}} (\text{\AA}) + 0.1504(d_{\text{O-H}\cdots\text{O}})^2 (\text{\AA}^2)$ , and  $|V(r)|/G(r) = 11.150 - 10.0071d_{\text{O-H}\cdots\text{O}} (\text{\AA}) + 2.4088(d_{\text{O-H}\cdots\text{O}})^2 (\text{\AA}^2)$ , for the polymorphs and TPPO cocrystals. These two equations are appealing since they are capable of connecting the experimental bond length ( $d_{\text{O-H}\cdots\text{O}}$ ) with the important theoretical descriptors like  $\rho_{\text{BCP}}$  and  $|V(r)|/G(r)$ . Thus, the empirical expressions provide us a gateway to access the electron density at BCP and also to distinguish the nature of H-bond interaction (closed-shell, intermediate, and covalent).

(iii) Correlation analysis between the  $E_{\text{SAPT0}}$  and  $\rho_{\text{BCP}}$  parameters has afforded an acceptable linear dependency,  $E_{\text{SAPT0}} (\text{kcal/mol}) = -381.28\rho_{\text{BCP}} (\text{a.u.}) - 1.578$ , with a MAPE of 9.26%. This empirical equation can be used to get a quick and reliable semiquantitative measurement of H-bond

interaction energy for any TPPO cocrystal. Therefore, only being provided with the donor–acceptor bond length can we estimate the H-bond interaction energy.

(iv) Both the parameters,  $|V(r)|/G(r)$  and  $H(r)/\rho(r)$  at BCP had been suggested by Espinosa et al. as a measure of covalent character in the H-bonds.<sup>36</sup> This study has given us an opportunity to check the efficacy of both the parameters, and we have found that the parameter  $|V(r)|/G(r)$  is much more effective than the  $H(r)/\rho(r)$  at BCP to gauge the extent of covalency in the H-bonds.

(v) We have found that all of the SAPT0 energy components correlate well with the respective interaction energies of the TPPO.H-bond donor compounds. To get a semiquantitative estimation of the individual SAPT0 energy terms, the linear equations given in Figure 4 can be employed for the TPPO cocrystals.

(vi) A measure of the noncovalent interaction energy can be alternatively fetched from IBSI. The equation,  $E_{\text{SAPT0}} (\text{kcal/mol}) = -2.383 - 214.87(\text{IBSI}) + 283.39(\text{IBSI})^2$ , helps us to discriminate covalent type interaction from the noncovalent class. We have been successful to link the theoretical descriptor IBSI with the experimental H-bond length via the relation,  $\text{IBSI} = 0.1652 - 1.203d^2_{\text{O-H}\cdots\text{O}} (\text{\AA}^{-2}) + 2.708(d^2_{\text{O-H}\cdots\text{O}})^2 (\text{\AA}^{-4})$ .

(vii) We have proposed two promising avenues for a fast semiquantitative calculation of the H-bond interaction energy from a nonenergetic observable, namely, the bond length:  $d_{\text{O-H}\cdots\text{O}} \rightarrow \rho_{\text{BCP}} \rightarrow E_{\text{SAPT0}}$ , and  $d_{\text{O-H}\cdots\text{O}} \rightarrow \text{IBSI} \rightarrow E_{\text{SAPT0}}$ . The successful execution of the two paths principally arises from the fact that the accumulation of electron density at the BCP between the donor and acceptor atoms is essentially related to the local bond stretching force constant between the two atoms.

(viii) Finally, we have been able to sort out an indicative energy scale to distinguish the nature of the O-H $\cdots$ O interactions existing in the TPPO cocrystals. Applying an IBSI threshold of 0.15 in the equation  $E_{\text{SAPT0}} (\text{kcal/mol}) = -2.383 - 214.87(\text{IBSI}) + 283.39(\text{IBSI})^2$  at maximum 9.66% MAPE, any O-H $\cdots$ O interaction having an energy in excess of  $-31.0$  kcal/mol can be regarded as an interaction transitioning into the covalent domain.

### 4. COMPUTATIONAL METHODS

All DFT calculations have been carried out with the help of Gaussian 16, Revision C.01 program.<sup>49</sup> The DFT computations have been accomplished by employing a highly parametrized, empirical exchange–correlation functional with double the amount of nonlocal exchange (2X), i.e., the M06-2X functional<sup>50</sup> along with the def2-TZVP basis set.<sup>51</sup> The dispersion correction has been done with the Grimme dispersion correction functions<sup>52</sup> (D3). Succinctly, the study was performed at the M06-2X-D3/def2-TZVP level of theory. We have uniformly used the crystallographic coordinates in Cartesian form as obtained from olex2–1.5 program<sup>53</sup> for the theoretical analysis of the noncovalent interactions in all the polymorphs and cocrystals to ensure the restoration of crystal environment as much as possible. Cartesian coordinates of the TPPO.hemihydrate polymorphs, TPPO cocrystals, and anhydrous TPPO have been furnished in Tables S1–S18. The same functional and basis set have been utilized to calculate all the single-point (SP) energies. The Gauss-View 6.0 graphical interface<sup>54</sup> has been used to create the input files as well as to interpret the outcomes. The NBO and QTAIM analyses have

been performed through the NBO 3.1 program<sup>55</sup> as implemented in the Gaussian package and the Multiwfn 3.8 software,<sup>56</sup> respectively, at the M06-2X-D3/def2-TZVP level of theory. To obtain a quantitative idea about the fundamental energy components (induction, dispersion, exchange, and electrostatic) involved in the O–H...O interactions, decomposition of the interaction energy has been performed by the SAPT0 method using the correlation consistent aug-cc-pVDZ basis set<sup>57</sup> through the PSI4 electronic structure program<sup>58</sup> package. The fchk files obtained from Gaussian 16, Revision C.01 program have been used in the ultrafine integration grid as embedded in the Multiwfn 3.8 software for the IBSI calculations.<sup>59</sup>

## ■ ASSOCIATED CONTENT

### SI Supporting Information

The Supporting Information is available free of charge at <https://pubs.acs.org/doi/10.1021/acsomega.4c02658>.

Olex2-1.5 derived Cartesian coordinates for the O–H...O interactions observed in the TPPO.hemihydrate polymorphs (Tables S1–S4), TPPO cocrystals (Tables S5–S17), anhydrous TPPO (Table S18), and details of empirically calculated H-bond interaction energy values (Table S19) (PDF)

## ■ AUTHOR INFORMATION

### Corresponding Authors

**Jishnunil Chakraborty** – Department of Chemistry, St. Paul's Cathedral Mission College, University of Calcutta, Kolkata 700009, India; Email: [jishnunil@yahoo.co.in](mailto:jishnunil@yahoo.co.in)

**Jaydip Gangopadhyay** – Department of Chemistry, St. Paul's Cathedral Mission College, University of Calcutta, Kolkata 700009, India; [orcid.org/0000-0003-2328-2701](https://orcid.org/0000-0003-2328-2701); Email: [gjaydip@rediffmail.com](mailto:gjaydip@rediffmail.com)

### Authors

**Suphal Sen** – School of Applied Material Sciences, Central University of Gujarat, Gandhinagar, Gujarat 382030, India; [orcid.org/0009-0009-0455-6640](https://orcid.org/0009-0009-0455-6640)

**Ankita Sinha** – Department of Chemistry, St. Paul's Cathedral Mission College, University of Calcutta, Kolkata 700009, India; [orcid.org/0009-0002-4165-242X](https://orcid.org/0009-0002-4165-242X)

**Suparna Banerjee** – Department of Chemistry, Uluberia College, University of Calcutta, Howrah 711315, India; [orcid.org/0009-0000-6339-093X](https://orcid.org/0009-0000-6339-093X)

**Snehasish Debnath** – Analytical & Environmental Science Division and Centralized Instrument Facility, CSIR-CSMCRI, Bhavnagar, Gujarat 364002, India

**Aniruddha Ghosh** – Department of Chemistry, St. Paul's Cathedral Mission College, University of Calcutta, Kolkata 700009, India

Complete contact information is available at: <https://pubs.acs.org/doi/10.1021/acsomega.4c02658>

### Notes

The authors declare no competing financial interest.

## ■ ACKNOWLEDGMENTS

Since no funding has been received to carry out this research, we sincerely thank St. Paul's Cathedral Mission College, Kolkata, for providing the essential infrastructural facilities and other resources. We thankfully acknowledge Prof. James B.

Foresman from York college of Pennsylvania for his suggestion regarding computation and Prof. Subhendu kanjilal, Department of Mathematics of St. Paul's Cathedral Mission College for helpful discussion regarding regression analysis. J.G. likes to express his deep sense of gratitude to Swami Divyananda Maharaj, Ex-Principal of RKMVCC, Kolkata and Prof. Amalesh Banerjee, Ex-HOD of Economics of Rabindra Bharati University, Kolkata. Although the duo are not the subject experts, but they remain the imperishable flashes of inspiration to J.G. for their nobility. Not the least, J.G. wholeheartedly admires the constant motivation received from his daughter Adrija.

## ■ REFERENCES

- (1) Etter, M. C.; Baures, P. W. Triphenylphosphine oxide as a crystallization aid. *J. Am. Chem. Soc.* **1988**, *110*, 639–640.
- (2) Solomos, M. A.; Mohammadi, C.; Urbelis, J. H.; Koch, E. S.; Osborne, R.; Usala, C. C.; Swift, J. A. Predicting Cocrystallization Based on Heterodimer Energies: The Case of *N,N'*-Diphenylureas and Triphenylphosphine Oxide. *Cryst. Growth Des.* **2015**, *15*, 5068–5074.
- (3) Vishweshwar, P.; McMahon, J. A.; Bis, J. A.; Zaworotko, M. J. Pharmaceutical co-crystals. *J. Pharm. Sci.* **2006**, *95*, 499–516.
- (4) Schultheiss, N.; Newman, A. Pharmaceutical Cocrystals and Their Physicochemical Properties. *Cryst. Growth Des.* **2009**, *9*, 2950–2967.
- (5) Bolton, O.; Matzger, A. J. Improved stability and smart material functionality realized in an energetic cocrystal. *Angew. Chem., Int. Ed.* **2011**, *50* (38), 8960–8963.
- (6) Landenberger, K. B.; Bolton, O.; Matzger, J. A. Energetic-Energetic Cocrystals of Diacetone Diperoxide (DADP): Dramatic and Divergent Sensitivity Modifications via Cocrystallization. *J. Am. Chem. Soc.* **2015**, *137*, 5074–5079.
- (7) Arnett, E. M.; Mitchell, E. J.; Murty, T. S. S. R. Basicity. Comparison of hydrogen bonding and proton transfer to some Lewis bases. *J. Am. Chem. Soc.* **1974**, *96*, 3875–3891.
- (8) D. Hadzi, D.; Smerkolj, R. Hydrogen bonding in some adducts of oxygen bases with acids. Part 8.-Proton chemical shifts and thermodynamic data on the association of chloroacetic acids with some oxygen bases. *J. Chem. Soc., Faraday Trans.* **1976**, *1*, 1188–1191.
- (9) Baures, P. W.; Silverton, J. V. Structure of Triphenylphosphine Oxide Hemihydrate. *Acta Crystallogr.* **1990**, *C46*, 715–717.
- (10) Baures, P. W. Monoclinic Triphenylphosphine Oxide Hemihydrate. *Acta Crystallogr.* **1991**, *C47*, 2715–2716.
- (11) Ng, S. W. A second monoclinic modification of triphenylphosphine oxide hemihydrate. *Acta Crystallogr.* **2009**, *E65*, o1431.
- (12) Desiraju, G. R. Supramolecular Synthons in Crystal Engineering-A New Organic Synthesis. *Angew. Chem., Int. Ed. Engl.* **1995**, *34*, 2311–2327.
- (13) Roşca, S.; Olaru, M.; Raţ, C. I. (2,4,6-Trimethylphenyl)boronic acid–triphenylphosphine oxide (1/1). *Acta Crystallogr.* **2012**, *E68*, o31.
- (14) Fuquen, R. M.; Valderrama-N, J.; Shankland, K.; Fabbiani, F. P. A.; Markvardsen, A. J. Three-centre hydrogen bonds in triphenylphosphine oxide–hydroquinone (1/1). *Acta Crystallogr.* **2008**, *64* (2), o367.
- (15) Al-Farhan, K. A. Triphenylphosphine oxide-1-naphthoic acid (1/1). *Acta Crystallogr.* **2004**, *C60*, o531–o532.
- (16) Al-Farhan, K. A. Triphenylphosphine oxide–3-chlorobenzoic acid (1/1). *Acta Crystallogr.* **2003**, *C59*, o179–o180.
- (17) Fuquen, R. M.; Lechat, J. R. Structure of the 1: 1 complex formed by triphenylphosphine oxide and 4-nitrophenol. *Acta Crystallogr.* **1992**, *C48*, 1690–1692.
- (18) Ahn, S. H.; Cluff, K. J.; Bhuvanesh, N.; Blümel, J. Hydrogen Peroxide and Di(hydroperoxy)propane Adducts of Phosphine Oxides as Stoichiometric and Soluble Oxidizing Agents. *Angew. Chem., Int. Ed.* **2015**, *54* (45), 13341–13345.

- (19) Batt, R. V.; Bullivant, D. P.; Elkington, K. E.; Hill, S. E.; Hilton, J.; Houghton, T. J.; Hovell, M.; Wallwork, S. C. The crystal structure of the nitric acid adducts of triphenylarsine oxide and triphenylphosphine oxide. *Polyhedron* **1998**, *17*, 2173–2178.
- (20) Takahashi, I.; Takahashi, Y.; Hatanaka, M.; Yamano, A.; Ohta, T.; Hosoi, S. Crystal Structure of a Complex Formed from Triphenylphosphine Oxide and 6-Chloro-2-pyridone. *Anal. Sci* **2002**, *18*, 1407–1408.
- (21) Thor, G.; Husebye, S.; Maartmann-Moe, K. Crystal structure of the Hydrogen-bonded complex between Pentafluorophenol and Triphenylphosphine oxide. *Acta Chem. Scand., Ser. B* **1986**, *40*, 26–30.
- (22) Lynch, D. E.; Smith, G.; Calos, N. J.; Kennard, C. H.; Whittaker, A. K.; Jack, K. S.; Willis, A. C. Molecular Cocrystals of Carboxylic Acids. XIII. Spectral Characterization of the Adducts of Triphenylphosphine Oxide With Substituted Benzoic Acids and the Crystal Structures of the 1: 1 Adducts With 2,4,6-Trinitrobenzoic Acid and 3,5-Dinitrobenzoic Acid. *Aust. J. Chem.* **1993**, *46*, 1535–1543.
- (23) Lariucci, C.; Santos, R. H. A.; Lechat, J. R. Structure of the 1: 1 adduct formed by diphenylmethanol with triphenylphosphine oxide. *Acta Crystallogr.* **1986**, *42* (12), 1825–1828.
- (24) Bader, R. F. W. *Atoms in Molecules, a Quantum Theory*; Oxford University Press: Oxford, UK, 1990.
- (25) *Quantum Theory of Atoms in Molecules: recent Progress in Theory and Application*, Matta, C.; Boyd, R. J., Ed.; Wiley-VCH Weinheim: Germany, 2007.
- (26) Klein, J.; Khartabil, H.; Boisson, J.-C.; Contreras-García, J.; Piquemal, J.-P.; Hénon, E. New Way for Probing Bond Strength. *J. Phys. Chem. A* **2020**, *124*, 1850–1860.
- (27) Weinhold, F.; Landis, C. *Valency and Bonding, a Natural Bond Orbital Donor-Acceptor Perspective*; Cambridge University Press: Cambridge, UK, 2005.
- (28) Reed, R.; Curtiss, L. A.; Weinhold, F. Intermolecular interactions from a natural bond orbital, donor-acceptor viewpoint. *Chem. Rev.* **1988**, *88*, 899–926.
- (29) Jeziorski, B.; Moszynski, R.; Szalewicz, K. Perturbation theory approach to intermolecular potential energy surfaces of van der Waals complexes. *Chem. Rev.* **1994**, *94*, 1887–1930.
- (30) Bader, R. F. W.; Nguyen-Dang, T. T.; Tal, Y. A topological theory of molecular structure. *Rep. Prog. Phys.* **1981**, *44*, 893–948.
- (31) Bader, R. F. W.; Beddall, P. M. Virial field relationship for molecular charge distributions and the spatial partitioning of molecular properties. *J. Chem. Phys.* **1972**, *56*, 3320–3329.
- (32) Bader, R. F. W. Comment on the Comparative Use of the Electron Density and Its Laplacian. *Chem. — Eur. J.* **2006**, *12*, 7769–7772.
- (33) Popelier, P. L. A. On the full topology of the Laplacian of the electron density. *Coord. Chem. Rev.* **2000**, *197*, 169–189.
- (34) Bader, R. F. W.; Essen, H. The characterization of atomic interactions. *J. Chem. Phys.* **1984**, *80*, 1943–1960.
- (35) Bone, R. G. A.; Bader, R. F. W. Identifying and analyzing intermolecular bonding interactions in van der Waals molecules. *J. Phys. Chem.* **1996**, *100*, 10892–10911.
- (36) Espinosa, E.; Alkorta, I.; Elguero, J.; Molins, E. From weak to strong interactions: A comprehensive analysis of the topological and energetic properties of the electron density distribution involving X–H...F–Y systems. *J. Chem. Phys.* **2002**, *117*, 5529–5542.
- (37) Parker, T. M.; Burns, L. A.; Parrish, R. M.; Ryno, A. G.; Sherrill, C. D. Levels of symmetry adapted perturbation theory (SAPT). I. Efficiency and performance for interaction energies. *J. Chem. Phys.* **2014**, *140* (9), 094106.
- (38) Brdarski, S.; Karlstrom, G. Modeling of the Exchange Repulsion Energy. *J. Phys. Chem. A* **1998**, *102*, 8182–8192.
- (39) Espinosa, E.; Molins, E.; Lecomte, C. Hydrogen bond strengths revealed by topological analyses of experimentally observed electron densities. *Chem. Phys. Lett.* **1998**, *285* (3–4), 170–173.
- (40) Emamian, S.; Lu, T.; Kruse, H.; Emamian, H. Exploring Nature and Predicting Strength of Hydrogen Bonds: A Correlation Analysis Between Atoms-in Molecules Descriptors, Binding Energies, and Energy Components of Symmetry-Adapted Perturbation Theory. *J. Comput. Chem.* **2019**, *40*, 2868–2881.
- (41) Mulliken, R. S.; Person, W. B. *Molecular Complexes*; Wiley: New York, 1969.
- (42) Thomas, J. A.; Hamor, T. A. Structure of orthorhombic triphenylphosphine oxide: a redetermination at room temperature. *Acta Crystallogr.* **1993**, *C49*, 355–357.
- (43) Lefebvre, C.; Rubez, G.; Khartabil, H.; Boisson, J.-C.; Contreras-García, J.; Hénon, E. Accurately extracting the signature of intermolecular interactions present in the NCI plot of the reduced density gradient versus electron density. *Phys. Chem. Chem. Phys.* **2017**, *19*, 17928–17936.
- (44) Lefebvre, C.; Khartabil, H.; Boisson, J.-C.; Contreras-García, J.; Piquemal, J.-P.; Hénon, E. The Independent Gradient Model: A New Approach for Probing Strong and Weak Interactions in Molecules from Wave Function Calculations. *ChemPhyschem* **2018**, *19*, 724–735.
- (45) Mulliken, R. Electronic Population Analysis on LCAOMO Molecular Wave Functions. I. *J. Chem. Phys.* **1955**, *23*, 1833–1840.
- (46) Wiberg, K. A. Application of the pople-santry-segal CNDO method to the cyclopropylcarbiny and cyclobutyl cation and to bicyclobutane. *Tetrahedron* **1968**, *24*, 1083–1096.
- (47) Mayer, I. Charge, bond order and valence in the AB initio SCF theory. *Chem. Phys. Lett.* **1983**, *97*, 270–274.
- (48) Mayer, I. Bond order and valence indices: A personal account. *J. Comput. Chem.* **2007**, *28*, 204–221.
- (49) Frisch, M. J.; Trucks, G. W.; Schlegel, H. B.; Scuseria, G. E.; Robb, M. A.; Cheeseman, J. R.; Scalmani, G.; Barone, V.; Petersson, G. A.; Nakatsuji, H., et al. *GAUSSIAN 16, Revision C.01*; Gaussian, Inc.: Wallingford CT, 2019.
- (50) Zhao, Y.; Truhlar, D. G. The M06 suite of density functionals for main group thermochemistry, thermochemical kinetics, non-covalent interactions, excited states, and transition elements: two new functionals and systematic testing of four M06-class functionals and 12 other functionals. *Theor. Chem. Acc.* **2008**, *120*, 215–241.
- (51) Weigend, F.; Ahlrichs, R. Balanced basis sets of split valence, triple zeta valence and quadruple zeta valence quality for H to Rn: Design and assessment of accuracy. *Phys. Chem. Chem. Phys.* **2005**, *7*, 3297–3305.
- (52) Grimme, S.; Antony, J.; Ehrlich, S.; Krieg, H. A. A consistent and accurate *ab initio* parametrization of density functional dispersion correction (DFT-D) for the 94 elements H–Pu. *J. Chem. Phys.* **2010**, *132* (15), 154104.
- (53) Dolomanov, O. V.; Bourhis, L. J.; Gildea, R. J.; Howard, J. A. K.; Puschmann, H. OLEX2: a complete structure solution, refinement and analysis program. *J. Appl. Crystallogr.* **2009**, *42*, 339–341.
- (54) *GaussView 6.0*; Gaussian Inc.: Wallingford, CT, USA, 2017.
- (55) Glendening, E. D.; Reed, A. E.; Carpenter, J. E.; Weinhold, F. *NBO Version 3.1*; TCI, University of Wisconsin: Madison, 1998.
- (56) Lu, T.; Chen, F. Multiwfn: A multifunctional wavefunction analyzer. *J. Comput. Chem.* **2012**, *33*, 580–592.
- (57) Dunning Jr, T. H. Gaussian basis sets for use in correlated molecular calculations. I. The atoms boron through neon and hydrogen. *J. Chem. Phys.* **1989**, *90*, 1007–1023.
- (58) Turney, J. M.; Simmonett, A. C.; Parrish, R. M.; Hohenstein, E. G.; Evangelista, F. A.; Fermann, J. T.; Mintz, B. J.; Burns, L. A.; Wilke, J. J.; Abrams, M. L.; et al. *PSI4: An Open-Source Ab Initio Electronic Structure Program. WIREs Comput. Mol. Sci.* **2012**, *2*, 556–565.
- (59) Šivickyte, O.; Costa, P. J. Intrinsic bond strength index as a halogen bond interaction energy predictor. *Phys. Chem. Chem. Phys.* **2023**, *25*, 17535–17546.